Constraining the Cosmological Constant from Large-Scale Redshift-Space Clustering

Takahiko Matsubara

Department of Physics and Astrophysics, Nagoya University, Chikusa, Nagoya 464-8602, Japan

and

Alexander S. Szalay

Department of Physics and Astronomy, The Johns Hopkins University, Baltimore, MD 21218

`taka@a.phys.nagoya-u.ac.jp, szalay@jhu.edu`

ABSTRACT

We show how the cosmological constant can be estimated from redshift surveys at different redshifts, using maximum-likelihood techniques. The apparent redshift-space clustering on large scales ($\gtrsim 20\ h^{-1}\mathrm{Mpc}$) are affected in the radial direction by infall, and curvature influences the apparent correlations in the transverse direction. The relative strengths of the two effects will strongly vary with redshift. Using a simple idealized survey geometry, we compute the smoothed correlation matrix of the redshift-space correlation function, and the Fisher matrix for Ω_{M} and Ω_{Λ}. These represent the best possible measurement of these parameters given the geometry. We find that the likelihood contours are turning, according to the behavior of the angular-diameter distance relation. The clustering measures from redshift surveys at intermediate-to-high redshifts can provide a surprisingly tight constraint on Ω_{Λ}. We also estimate confidence contours for real survey geometries, using the SDSS LRG and QSO surveys as specific examples. We believe that this method will become a practical tool to constrain the nature of the dark energy.

Subject headings: cosmology: theory —galaxy clustering — large-scale structure of universe

1. Introduction

The dark energy, which is the cosmological constant Λ in its simplest form, currently have turned out to possibly be a dominant component in the universe (e.g., Bahcall et al. 1999). It is one of the central issues in cosmology to reveal the quantitative nature of this mysterious form of the energy. One of the mysteries of the cosmological constant is its smallness. There are no evidence

detected on the Earth for existence of the cosmological constant. The cosmological constant is so small that it only affects the phenomena on cosmologically large scales.

There are several traditional tests of the cosmological constant. The expected frequency of multiple image lensing events for high-redshift sources is quite sensitive to the cosmological constant (Fukugita, Futamase, & Kasai 1990; Turner 1990). Luminosity–volume, and redshift–volume relations can also be used to measure the geometry of the universe to constrain the cosmological constant (Rowan-Robinson 1968; Loh 1988). Alcock & Paczyński (1979) proposed an evolution-free test for the cosmological constant using statistically spherical objects. The type Ia supernova Hubble diagram is used to constrain the mass density parameter and the cosmological constant (Schmidt et al. 1998; Perlmutter et al. 1999) through the luminosity distance d_L. Acoustic peaks of Cosmic Microwave Background (CMB) anisotropies constrain the curvature of the universe (e.g., Hu, Sugiyama & Silk 1997). Recent observational developments of the type Ia supernova and the CMB anisotropies (Balbi et al. 2000; de Bernardis et al. 2000) suggest a flat, low-density universe with positive cosmological constant, $\Omega_M \sim 0.3, \Omega_\Lambda \sim 0.7$.

The effect of a cosmological constant on the clustering properties of objects in the nearby universe ($z \ll 1$) is so weak, that redshift surveys have not been used to constrain Ω_Λ so far. As the depth and the sampling rate of redshift surveys increase, redshift-space clustering depends on the cosmological constant through *the cosmological redshift distortions* (Ballinger, Peacock & Heavens 1996; Matsubara & Suto 1996; Matsubara 2000). Several applications of this effect are proposed (Nair 1999; Nakamura, Matsubara & Suto 1998; Popowski et al. 1998; Yamamoto & Suto 1999; Yamamoto, Nishioka & Suto 1999). To maximally extract the cosmological information from the survey data, the likelihood analysis combined with a data reduction technique like the Karhunen-Loève transform has been quite successful at low redshifts (Vogeley & Szalay 1996; Szalay, Matsubara & Landy 1998; Matsubara, Szalay & Landy 2000). We expect it to be just as useful at intermediate-to-high redshifts here.

In this *Letter*, we combine the two methods, i.e., the likelihood analysis on pixelized data and the cosmological distortions. Specifically, we compute the Fisher matrix for simple geometries to illustrate how the cosmological distortions constrain the cosmological constant and the density parameter in a given redshift survey data.

2. From Correlations to Fisher Matrix

To generically investigate how a given redshift survey can constrain the cosmological constant, we construct a rectangular box, in which objects like galaxies or quasars in redshift space are observed. We will use smooth pixels rather than hard cells in order to make our calculations numerically more efficient. We apply a Gaussian smoothing window to the objects in the survey, to get a smoothed estimate of the local density. With a sufficiently large smoothing radius, we do not have to deal with the nonlinearities of the density field. The Gaussian smoothed cells are placed

on lattice sites in the box. In this way, the smoothed density vector ρ_i on discrete lattice sites labeled by i is considered as our fundamental data to be analyzed. In the following we assume the mean value of the density vector $\langle\rho_i\rangle$ is known so that we can define a density-fluctuation vector $d_i = \rho_i/\langle\rho_i\rangle - 1$.

In standard theories of structure formation, the linear density field is a random Gaussian process. In this case, all clustering properties of the universe are represented by two-point correlations. Thus, a correlation matrix

$$C_{ij} = \langle d_i d_j \rangle, \tag{1}$$

theoretically specifies all the statistical information for a given data set. This matrix is related to a smoothed two-point correlation function plus a shot noise term:

$$C_{ij} = \int d^3 s_1 \, d^3 s_2 \, W(\boldsymbol{s}_i - \boldsymbol{s}_1) W(\boldsymbol{s}_j - \boldsymbol{s}_2) \, \xi(\boldsymbol{s}_1, \boldsymbol{s}_2) + \int d^3 s \, W(\boldsymbol{s}_i - \boldsymbol{s}) W(\boldsymbol{s}_j - \boldsymbol{s})/\bar{n}(\boldsymbol{s}), \tag{2}$$

where $W(\boldsymbol{s}) = \exp[-s^2/(2R^2)]/(\sqrt{2\pi}R)$ is a Gaussian smoothing window, ξ is a two-point correlation function, and $\boldsymbol{s}_i$ is the position vector of a lattice site i, and $\bar{n}(\boldsymbol{s})$ is the mean number density field. The position vectors are all in observable redshift space which consists of the redshift z and the angular position (θ, ϕ). In the distant-observer approximation, we can approximately use the Cartesian coordinates in redshift space and the two-point correlation function is a function of the relative vector $\boldsymbol{s}_1 - \boldsymbol{s}_2$. The correlation function does depend on the direction of this relative vector, because of the redshift distortions. An analytic form of the linear two-point correlation function in redshift space including high-redshift effects is given by Matsubara & Suto (1996). One of the equivalent forms given in Matsubara & Suto (1996) is (see also Ballinger, Peacock & Heavens 1996)

$$\xi(\boldsymbol{s}_1 - \boldsymbol{s}_2) = b^2(z) D^2(z) \int \frac{d^3 k}{(2\pi)^3} e^{i\boldsymbol{k}\cdot(\boldsymbol{x}_1 - \boldsymbol{x}_2)} \left[1 + \beta(z) k_3{}^2/k^2\right]^2 P(k), \tag{3}$$

where $P(k)$ is the linear mass power spectrum at $z = 0$, $D(z)$ is the linear growth rate normalized as $D(0) = 1$, $b(z)$ is the bias factor at redshift z, and $\beta(z)$ is the redshift distortion parameter, which is approximately related to the redshift-dependent mass density parameter as $\beta(z) \sim \Omega_{\mathrm{M}}{}^{0.6}(z)/b(z)$. In the above equation, the third axis is taken as the direction of the line of sight. The vectors $\boldsymbol{x}_1$ and $\boldsymbol{x}_2$ are the comoving positions of the two points which are labeled by $\boldsymbol{s}_1$ and $\boldsymbol{s}_2$ in redshift space (see Matsubara & Suto 1996), i.e., they are related by a comoving distance–redshift relation and the spatial curvature of the universe. Assuming the distant-observer approximation, a Gaussian window function, and that the mean number density is effectively constant, $\bar{n}$, the equation (2) finally reduces to

$$\begin{aligned} C_{ij} = {}&\frac{1}{2} b^2(z) D^2(z) \int_0^\infty \frac{k^2 dk}{2\pi^2} P(k) \int_0^\pi \sin\theta d\theta \exp\left\{-k^2 R^2 \left[\left(c_\parallel{}^2 - c_\perp{}^2\right)\cos^2\theta + c_\perp{}^2\right]\right\} \\ &\times \left(1 + \beta\cos^2\theta\right)^2 J_0\left(kx\sin\theta_x\sin\theta\right)\cos\left(kx\cos\theta_x\cos\theta\right) \\ &+ \frac{\exp\left[-x^2/(4R^2)\right]}{\pi^{3/2}(2R)^3\bar{n}} \end{aligned} \tag{4}$$

In this equation, $c_\parallel(z) = H_0/H(z)$, $c_\perp(z) = H_0 s_K(z)/z$ are the distortion factor parallel and perpendicular to the line of sight, respectively, where $H(z)$ and $s_K(z)$ are the Hubble parameter and the comoving angular diameter distance at z, and H_0 is the Hubble's constant. A line-of-sight component of the redshift-space distance $s_\parallel$ between the centers of i-cell and j-cell is related to that of the comoving distance $x_\parallel$ by $x_\parallel = c_\parallel(z)s_\parallel$. Similarly, for a component perpendicular to the line-of-sight we have $x_\perp = c_\perp(z)s_\perp$. In this notation, the quantities in equation (4) can be written as $x \equiv (c_\parallel{}^2 s_\parallel{}^2 + c_\perp{}^2 s_\perp{}^2)^{1/2}$, and $\theta_x = \cos^{-1}(c_\parallel s_\parallel/x)$. Integration over θ remains because a spherical Gaussian smoothing kernel in observable redshift space is no longer spherical but is ellipsoidal in comoving space. The second term in equation (4) is a shot noise term, convolved with the Gaussian kernel.

Once the correlation matrix can be theoretically calculated in any cosmological model, one can calculate the Cramér-Rao bound which gives an estimate how well the model parameters can be measured. This is one of the most powerful results in estimation theory (Therrien 1992). The Fisher information matrix is a key quantity in this theory (Kendall & Stuart 1969):

$$F_{\alpha\beta} = -\left\langle \frac{\partial^2 \ln L}{\partial\theta_\alpha \partial\theta_\beta} \right\rangle, \tag{5}$$

where $L(\boldsymbol{d}; \boldsymbol{\theta})$ is a probability distribution for the data vector $\boldsymbol{d}$, which depends on a vector of model parameters $\boldsymbol{\theta}$. In our case, the data vector is density fluctuations on lattice sites and the model parameters are the cosmological parameters. The Cramér-Rao bound states that the maximal likelihood estimate constrains the model parameters with a minimum variance

$$\langle \theta_\alpha \theta_\beta \rangle \geq \left(F^{-1}\right)_{\alpha\beta}, \tag{6}$$

where F^{-1} is the inverse matrix of F. When the number of data, i.e., the dimension of the data vector is very large, the Cramér-Rao bound (6) becomes equality. A contour $[\theta_\alpha F_{\alpha\beta} \theta_\beta]^{1/2} = A$ in parameter space gives a concentration ellipsoid, which indicate regions where the likelihood density for model parameters are most concentrated. The threshold $A = 1, 2, 3$ corresponds to maximally attainable confidence levels of 1σ, 2σ, 3σ, respectively, in a likelihood analysis, if the likelihood function is Gaussian. The concentration ellipsoids are useful even when the likelihood function is not Gaussian to give a rough idea of the spread of the density (Therrien 1992).

As we are interested in a linear density field, the probability distribution of the density field is considered to be Gaussian so that the likelihood function has the form,

$$-2\ln L = \ln \det \boldsymbol{C} + \boldsymbol{d}^T \boldsymbol{C}^{-1} \boldsymbol{d} + \text{const.} \tag{7}$$

where $\boldsymbol{C}$ is the correlation matrix which depends on model parameters, and $\boldsymbol{d}$ is the data vector. In this case, the Fisher information matrix reduces to (see, i.e., Vogeley & Szalay 1996)

$$F_{\alpha\beta} = \frac{1}{2}\text{Tr}\left(\boldsymbol{C}^{-1}\boldsymbol{C}_{,\alpha}\boldsymbol{C}^{-1}\boldsymbol{C}_{,\beta}\right), \tag{8}$$

where $\boldsymbol{C}_{,\alpha} = \partial\boldsymbol{C}/\partial\theta_\alpha$, etc. Thus, the Fisher matrix or the concentration ellipsoids for any model parameters are straightforward to calculate from the correlation matrix of equation (4).

3.   Results for a Simple Cubic Box

In this *Letter*, the mass density parameter Ω_M and the normalized cosmological constant Ω_Λ, both at the present time, are the model parameters to be constrained. These parameters has the primary importance in high-redshift clustering distortions. For simplicity, the power spectrum $P(k)$ and the bias parameter $b(z)$, on which the correlation matrix of equation (4) also depends, are fixed throughout. We use the cold dark matter-type spectrum with a fixed shape parameter $\Gamma = 0.2$ and a fixed normalization $\sigma_8 = 1$. The growth factor $D(z)$ and the distortion parameter $\beta(z)$ are the functions of Ω_M and Ω_Λ. Throughout this *Letter*, we take a fiducial models $(\Omega_M, \Omega_\Lambda) = (0.3, 0.7)$ at which the Fisher matrix is evaluated.

Although the most natural choice of the length unit system would be comoving coordinate system, we should not use this system, because they are not actually observable in redshift surveys, and depend on the cosmological models which we are seeking. Thus, we use the coordinate system like (z, θ, ϕ) in polar coordinates. The clustering scale we are interested in is too small in figures when the distance is represented by z itself, so that we invent a new radial coordinate $s = cz/H_0 \simeq 2997.9\,z$, i.e., the linear extrapolation of distance-redshift relation for $z \ll 1$. For example, a redshift interval $\Delta z = 0.1$ around *any* redshift z corresponds to $\Delta s = 300$. Although the unit of this coordinate system is still $h^{-1}\mathrm{Mpc}$, we use a new notation $h^{-1}\mathrm{Mpc}_z$ to avoid a confusion with the comoving coordinate system.

In this coordinate system, a $200\,h^{-1}\mathrm{Mpc}_z$ cubic box is considered to obtain generic estimates for Cramér-Rao bound, and we compute the Fisher matrix for this sample, varying the mean redshift z of this box. The density fluctuations are sampled on regular $10 \times 10 \times 10$ lattice sites in the box. The Gaussian smoothing radius is set as $R = 10\,h^{-1}\mathrm{Mpc}_z$.

Figure 1 shows the concentration ellipses of the $200\,h^{-1}\mathrm{Mpc}_z$ box placed at redshift $z = 0$ to 6.0. The contour lines correspond to $A = 1, 2, 3$ which indicate the maximally attainable confidence levels of 1σ, 2σ, 3σ when one performs a likelihood analysis for these samples as we described in the previous section. The shot noise is neglected in this Figure, while it would be difficult to reduce shot noise for $z \geq 2$ in reality. As is well known, a low-redshift sample ($z \sim 0$) only constrains the mass density parameter through its dependence of the redshift distortion parameter $\beta \sim \Omega_M^{0.6}/b$. Increasing the mean redshift, the concentration ellipses rotates clockwise and the major axis becomes shorter, and thus the cosmological constant becomes constrained. The higher the mean redshift is, the more the cosmological constant is constrained. Around $z \sim 1.7$, the concentration ellipses begin to rotate counterclockwise. This is consistent with the fact that the angular diameter distance–redshift relation turns over at $z \sim 1.7$ in our fiducial model $(\Omega_M, \Omega_\Lambda) = (0.3, 0.7)$.

On one hand, the number density one can sample is smaller for high-redshift objects, which dilute the constraints on cosmological parameters. On the other hand, there is a larger volume to be sampled than for low-redshift objects. To obtain the concentration ellipses in realistic samples, one should take into account both the shot noise effect and the total volume in a given sample. We
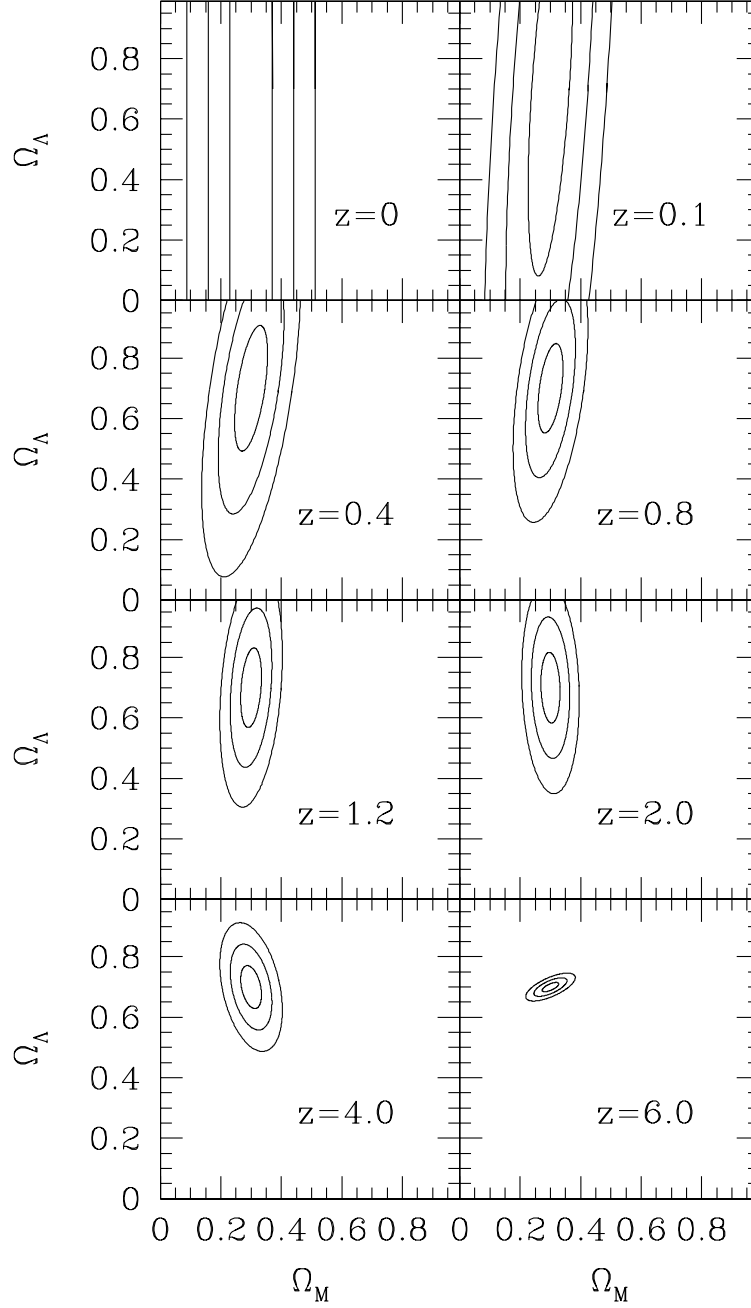
Fig. 1.— Concentration ellipses from the Fisher matrix for generic boxes. Contour lines correspond to confidence levels 1σ, 2σ, 3σ attainable from a single $200\,h^{-1}\mathrm{Mpc}_z$ box placed at redshift $z = 0$ to 6.0 as indicated in each panels. This figure contains no shot noise, and a bias factor of 1.

again set the $200\,h^{-1}\mathrm{Mpc}_z$ boxes and estimate the Cramér-Rao bound with the shot noise effect included. In Figure 2, the bound for the normalized cosmological constant Ω_Λ is plotted. In the left panel, the volume is given by just one $200\,h^{-1}\mathrm{Mpc}_z$ box as in the case of Figure 1. The shot noise is varied as $(20\,h^{-1}\mathrm{Mpc}_z)^3\bar{n} = 0.1, 0.3, 1, 3, 10$, and ∞, from top to bottom lines. In the right panel, the Cramér-Rao bound is scaled by the number of independent $200\,h^{-1}\mathrm{Mpc}_z$ boxes in a π steradian region with a redshift interval $z/2$ around z, to obtain a rough idea of how our error bound is affected by the survey volume. We can see how densely the objects should be sampled to constrain the cosmological constant with a certain accuracy both for a sample with a fixed volume and a sample with a fixed solid angle.

4.   Possibilities for Realistic Survey Volumes

We have considered several different survey layouts for both galaxies and quasars. The best survey to perform these tests seems to be the Luminous Red Galaxy (LRG) sample of the Sloan Digital Sky Survey (SDSS). This sample consists of 100,000 galaxies selected for spectroscopic observations on the basis of their very red rest frame colors, using photometric redshifts, down to a limiting magnitude of $r' = 19.5$. They form an approximately volume limited sample, where the outer edge lies at around $z = 0.45$, and the total surface area is 10,000 square degrees.

We consider this geometry as a composite of the generic $200\,h^{-1}\mathrm{Mpc}_z$ boxes at the mean redshift $z = 0.3$. There are about 220 boxes out to $z = 0.45$ in a π steradian region, so that the shot noise is approximately given by $(20\,h^{-1}\mathrm{Mpc}_z)^3\bar{n} = 0.5$. We assume two bias factors, $b = 1.5$ and $b = 2$. The resulting concentration ellipses are shown in Figure 3. We can see the result is quite remarkable. The Cramér-Rao bound for the cosmological constant is only $[(F^{-1})_{\Lambda\Lambda}]^{1/2} = 0.04$ for $b = 1.5$, and $[(F^{-1})_{\Lambda\Lambda}]^{1/2} = 0.03$ for $b = 2$. This shows that the shot noise level and the depth of the survey volume are suitably balanced to constrain the geometry of the universe in the SDSS LRG survey.

We have considered various QSO surveys to possibly measure the dark energy at higher redshifts. Unfortunately, the currently ongoing QSO redshift surveys, like Sloan Digital Sky Survey (SDSS, i.e., York et al. 2000) and 2dF QSO redshift survey (2QZ, i.e., Boyle et al. 2001), have lower sampling rates for QSOs, $\bar{n} \sim 10^{-3}/(40\,h^{-1}\mathrm{Mpc}_z)^3$. They typically give the Cramér-Rao bound of order $\Delta\Omega_\Lambda \sim 1$, almost regardless of the smoothing radius. To constrain the cosmological constant with QSO surveys, one should sample QSOs more densely than these current QSO surveys. This fact is in agreement with Popowski et al. (1998) who analyzed nonlinear clustering to constrain the geometry of the universe and indicated an advantage of a dense sampling.
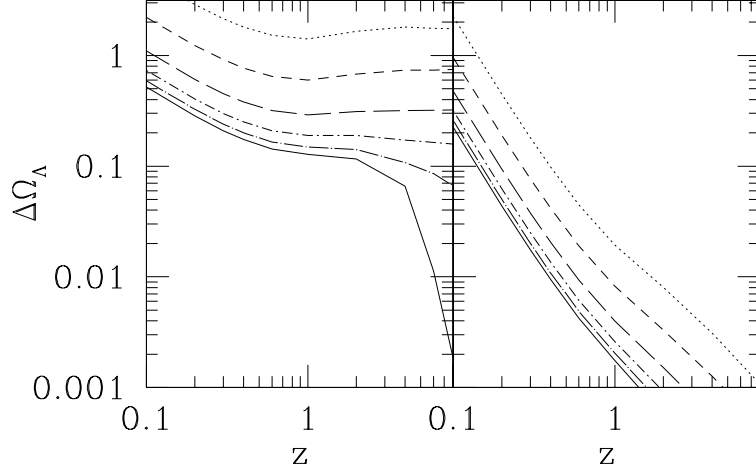
Fig. 2.— Cramér-Rao bound for the normalized cosmological constant Ω_Λ as a function of the mean redshift z. Shot noise is varied as $(20\,h^{-1}\mathrm{Mpc}_z)^3\bar{n} = 0.1, 0.3, 1, 3, 10$, and ∞, from top to bottom lines. *Left panel*: a single $200\,h^{-1}\mathrm{Mpc}_z$ box. *Right panel*: For a survey of π steradians, a redshift interval of $z/2$, centered at z. The number of independent boxes is increased by the volume of the shell, correspondingly the accuracy improves. A bias factor of 1 has been used throughout this figure.
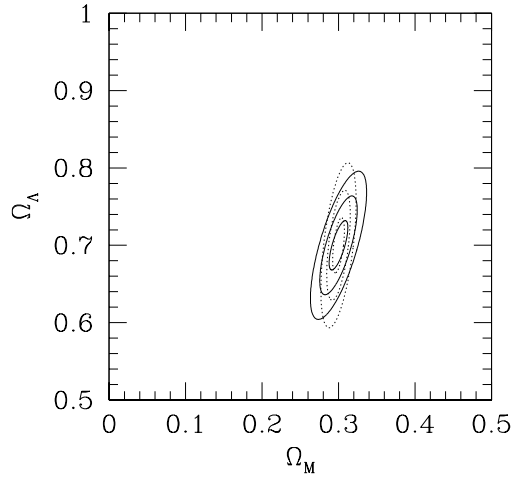

Fig. 3.— Concentration ellipses corresponding to 1σ, 2σ, 3σ confidence levels for approximate geometries of the 100,000 galaxies in the SDSS LRG (Luminous Red Galaxy) sample. Dotted lines assume a bias factor of $b = 1.5$, solid lines has $b = 2$.

5. Discussion

We have shown that large-scale clustering of galaxies at intermediate redshifts $z \sim 0.5$ is surprisingly suitable for constraining the cosmological parameters of Ω_M and Ω_Λ, and thus the geometry of the universe. The QSOs in currently ongoing surveys are too sparse to give comparable constraints.

The apparent redshift-space clustering method used in this *Letter* is a completely self-contained test for Ω_M and Ω_Λ. The results from this method can be further combined with any of the other independent tests to obtain stricter constraints, or to check a consistency of our standard picture of the cosmology.

One can use Figure 2 to aid designs of future surveys at various redshifts. The lines indicate the statistical uncertainty in the cosmological constant corresponding to different sampling rates. They should be scaled, noting that the Cramér-Rao error bound roughly scales as the inverse of the square of survey volumes.

In this work, we have only considered two parameters Ω_M and Ω_Λ. We still need to measure the evolution of bias parameter, which is not obvious. Moreover, there is a possiblity that the dark energy has a more complex behaviour than the cosmological constant (Wang et al. 2000). There are many other cosmological parameters, like baryonic density Ω_b, primordial spectral index n, the neutrino mass density Ω_ν, etc., which more or less depend on the apparent redshift-space clustering.

REFERENCES

Alcock, C. & Paczyński, B. 1979, Nature, 281, 358

Bahcall, N. A., Ostriker, J. P., Perlmutter, S., & Steinhardt, P. J. 1999, Science, 284, 1481

Balbi, A. et al. 2000, ApJ, 545, L1

Ballinger, W. E., Peacock, J. A. & Heavens, A. F. 1996, MNRAS, 282, 877

Boyle, B. J., Croom, S. M., Smith, R. J., Shanks, T., Outram, P. J., Hoyle, F., Miller, L. & Loaring, N. S. 2001, submitted to proceedings of ESO Deep Fields conference., (astro-ph/0103064)

de Bernardis, P. et al. 2000, Nature, 404, 955

Davis, M., Newman, J., Faber, S., & Phillips, A. 2000, to appear in Proc. of the ESO/ECF/STSCI workshop on Deep Fields, Garching Oct 2000, (astro-ph/0112189)

Fukugita, M., Futamase, T., & Kasai, M. 1990, MNRAS, 246, 24P

Hu, W., Sugiyama, N. & Silk, J. 1997, Nature, 386, 37

Kendall, M. G. & Stuart, A. 1969, The Advanced Theory of Statistics, Vol. 2 (London: Griffin)

Loh, E. D. 1988, ApJ, 329, 24

Matsubara, T. 2000, ApJ, 535, 1

Matsubara, T. & Suto, Y. 1996, ApJ, 470, L1

Matsubara, T., Szalay, A. S. & Landy, S. D. 2000, ApJ, 535, L1

Nair, V. 1999, ApJ, 522, 569

Nakamura, T. T., Matsubara, T., & Suto, Y. 1998, ApJ, 494, 13

Perlmutter, S. et al. 1999, ApJ, 517, 565

Popowski, P. A., Weinberg, D. H., Ryden, B. S. & Osmer, P. S. 1998, ApJ, 498, 11

Rowan-Robinson, M. 1968, MNRAS, 138, 445

Schmidt, B. P. et al. 1998, ApJ, 507, 46

Szalay, A. S., Matsubara, T. & Landy, S. D. 1998, ApJ, 498, L1

Therrien, C. W. 1992, Discrete Random Signals and Statistical Signal Processing, (New Jersey: Prentice-Hall).

Turner, E. L. 1990, ApJ, 365, L43

Vogeley, M. S. & Szalay, A. S. 1996, ApJ, 465, 34

Wang, L., Caldwell, R. R., Ostriker, J. P. & Steinhardt, P. J. 2000, ApJ, 530, 17

Yamamoto, K. & Suto, Y. 1999, ApJ, 517, 1

Yamamoto, K., Nishioka, H., & Suto, Y. 1999, ApJ, 527, 488

York, D. G. et al. 2000, AJ, 120, 1579